AGU PUBLICATIONS

Geophysical Research Letters

RESEARCH LETTER
10.1002/2017GL075697

Key Points:
- Constraints on the viscosity/thickness of the asthenosphere challenge the notion that subduction is the main driver of Pacific Plate motion
- We use coupled global models of mantle and lithosphere dynamics to simulate the dynamics of the Pacific Plate since 15 Ma
- Results indicate that a strong Poiseuille (i.e., pressure driven) component of asthenospheric flow drives >50% of the Pacific Plate motion

Supporting Information:
- Supporting Information S1

Correspondence to:
I. L. Stotz,
ilsc@ign.ku.dk

Citation:
Stotz, I. L., Iaffaldano, G., & Davies, D. R. (2018). Pressure-driven Poiseuille flow: A major component of the torque-balance governing Pacific Plate motion. *Geophysical Research Letters*, *45*, 117–125. https://doi.org/10.1002/2017GL075697

Received 15 SEP 2017
Accepted 6 DEC 2017
Accepted article online 12 DEC 2017
Published online 8 JAN 2018

Pressure-Driven Poiseuille Flow: A Major Component of the Torque-Balance Governing Pacific Plate Motion

I. L. Stotz[1], **G. Iaffaldano**[1], **and D. R. Davies**[2]

[1]Department of Geosciences and Natural Resource Management, University of Copenhagen, Copenhagen, Denmark, [2]Research School of Earth Sciences, Australian National University, Canberra, ACT, Australia

Abstract The Pacific Plate is thought to be driven mainly by slab pull, associated with subduction along the Aleutians-Japan, Marianas-Izu-Bonin, and Tonga-Kermadec trenches. This implies that viscous flow within the sub-Pacific asthenosphere is mainly generated by overlying plate motion (i.e., Couette flow) and that the associated shear stresses at the lithosphere's base are resisting such motion. Recent studies on glacial isostatic adjustment and lithosphere dynamics provide tighter constraints on the viscosity and thickness of Earth's asthenosphere and, therefore, on the amount of shear stress that asthenosphere and lithosphere mutually exchange, by virtue of Newton's third law of motion. In light of these constraints, the notion that subduction is the main driver of present-day Pacific Plate motion becomes somewhat unviable, as the pulling force that would be required by slabs exceeds the maximum available from their negative buoyancy. Here we use coupled global models of mantle and lithosphere dynamics to show that the sub-Pacific asthenosphere features a significant component of pressure-driven (i.e., Poiseuille) flow and that this has driven at least 50% of the Pacific Plate motion since, at least, 15 Ma. A corollary of our models is that a sublithospheric pressure difference as high as ±50 MPa is required across the Pacific domain.

1. Introduction

The Pacific Plate (PA) is currently the largest and fastest tectonic plate on Earth. It moves at an angular velocity of ~0.75°/Myr (e.g., Stotz et al., 2017; Wessel & Kroenke, 2008), which translates into surface velocities of 6–8.5 cm/yr along the great circle associated with the PA Euler pole.

Several studies have argued that the main driver of PA dynamics is slab pull, arising due to subduction along the Aleutians-Japan, Marianas-Izu-Bonin, and Tonga-Kermadec trenches (see Faccenna et al., 2012; Forsyth & Uyeda, 1975; Lallemand et al., 2005, and references therein). Under this scenario, ridge push forces provide a second-order contribution to the force balance (Fowler, 2004; Seno, 2000), and it is implied that slab pull overcomes both the resistance exerted by friction along shallow, brittle plate margins, and viscous stresses at the base of the plate (i.e., at the lithosphere-asthenosphere boundary). The key unknown remains the fraction of the net slab weight (i.e., the slab's negative buoyancy minus the viscous stresses acting along its surface) that is transmitted into pulling the trailing plate, with the remainder largely contributing to bending the lithosphere at the trench. Previous studies estimate this fraction to be anywhere from 20 to 80% of the net slab weight (e.g., Buffett & Becker, 2012; Capitanio et al., 2007; Conrad & Hager, 1999; Conrad & Lithgow-Bertelloni, 2002; Faccenna et al., 2012; Schellart, 2004).

Arguing that PA motion is principally driven by slab pull implies that Earth's asthenosphere is resisting PA motion and that the contribution of active asthenospheric flow (i.e., that driving plate motion) to PA dynamics is negligible (although Rowley et al. (2016) recently questioned such a notion on the basis of the dynamics of the East Pacific Rise). To first order, this can be described through a simple, 1-D linear force balance (Iaffaldano & Bunge, 2015) where a generic squared plate, whose side is L, glides over the asthenosphere at velocity v, pulled by a force F. Such a force, which in this simple example represents the pull exerted by subducting slabs onto the trailing plate (commonly referred to as slab pull), works against the integral of basal shear stresses at the plate base. The 1-D force balance is $F-\mu_A\cdot(v/H_A)\cdot L^2=0$, where μ_A is the viscosity of the asthenosphere and H_A is its thickness. A simple inversion of the force balance equation yields $F=v\cdot L^2\cdot(\mu_A/H_A)$. This means that the linear density of pulling force along one side of the plate is $F/L=v\cdot L\cdot(\mu_A/H_A)$. Thus, inverting the force balance

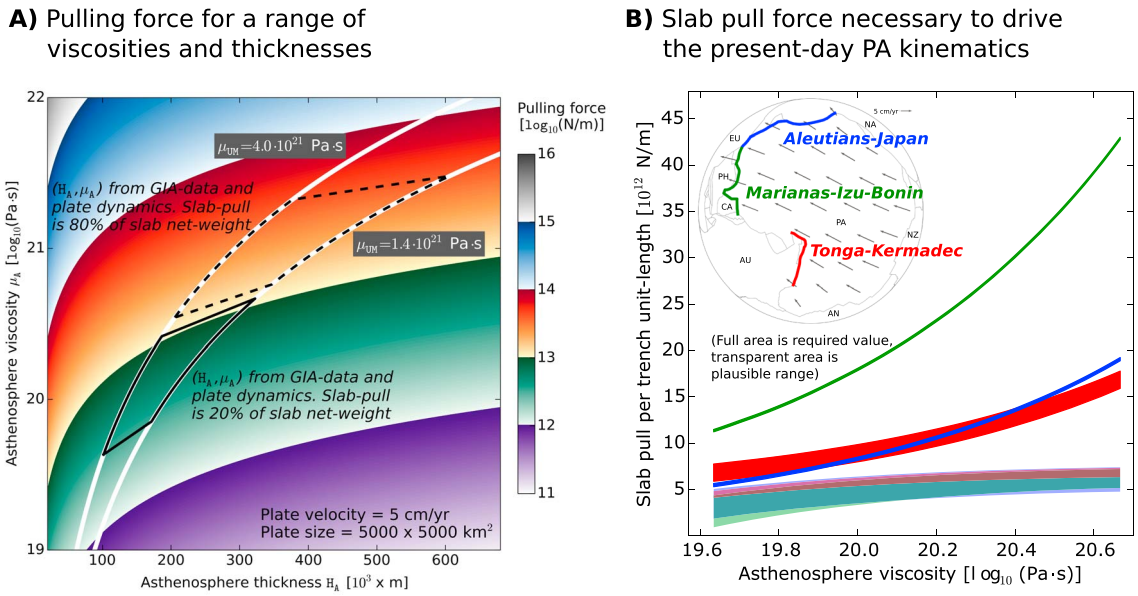

Figure 1. (a) Slab pull force inferred from the simple 1-D force balance of a tectonic plate (see main text) for a range of asthenospheric thickness (H_A) and viscosity (μ_A) values. Pairs (H_A, μ_A) within white lines are compatible with GIA constraints (Paulson & Richards, 2009). Black boxes show pairs (H_A, μ_A) also compatible with lithosphere dynamics constraints under the assumption that 20% (solid black) and 80% (dashed black) of the net slab weights transferred to the trailing plate (Iaffaldano & Lambeck, 2014). (b) Filled areas are values of slab pull required along the Tonga-Kermadec, Marianas-Izu-Bonin, and Aleutians-Japan trenches in order to drive the present-day PA motion (see map inset—NA is North American plate, EU is Eurasian plate, PH is Philippine Sea plate, CA is Caroline plate, AU is Australian plate, AN is Antarctica plate, and NZ is Nazca plate), under the assumption that the sub-Pacific asthenosphere passively resists such motion. Transparent areas are maximum plausible values of slab pull force available at each trench (see main text for further details).

in order to constrain plate-driving forces (e.g., slab pull) relies significantly on the ratio between the viscosity of Earth's asthenosphere and its thickness. Although motions and dimensions of present-day tectonic plates are reasonably well constrained from reconstructions of ocean floor magnetization (e.g., Gibbons et al., 2015), the viscosity and thickness of the asthenosphere are more uncertain, with independent estimates typically coming from rheological experiments on rock samples for the former (e.g., Karato, 2010, 2012), and upper mantle seismic tomography studies for the latter (e.g., Colli et al., 2014; French et al., 2013).

With reference to the simple 1-D force balance described above, Figure 1a shows the pulling force needed to drive a 5,000 × 5,000 km^2 plate at 5 cm/yr, over a wide range of asthenospheric viscosities and thicknesses. If one were to select these values independently from each other, then the inferred driving force could span several orders of magnitude (Figure 1a). In other words, treating the viscosity of the asthenosphere (μ_A) independently from its thickness (H_A) results in large uncertainties on inferences of plate-driving forces. However, recent analyses of glacial isostatic adjustment (GIA) data indicate that these two parameters are, in fact, linked to one another. In a notable study, Paulson and Richards (2009) demonstrate that the viscosity contrast between asthenosphere and the lower part of the upper mantle is proportional to the cube of the asthenosphere thickness. That is, the thicker the asthenosphere, the higher its viscosity needs to be to reconcile the average viscosity of the upper half of Earth's mantle with the Haskell value (Haskell, 1937; Mitrovica, 1996). Thick white lines in Figure 1a delineate the constraints provided by Paulson and Richards (2009) for two end-member values of lowermost upper mantle viscosity (μ_{UM}): any pair (H_A, μ_A) between these lines is compatible with GIA constraints, which reduces the uncertainty on the inference of the driving force to ~2 orders of magnitude.

Iaffaldano and Lambeck (2014) further narrowed the geodynamically plausible values of asthenosphere viscosity and thickness, by combining these constraints from GIA with the independently established notion that subduction initiation in the western Pacific, around the time of the Hawaiian-Emperor bend, caused the ~60° directional change of PA motion at that time (Faccenna et al., 2012; Wessel & Kroenke, 2008). Specifically, after assuming that the slab pull is a given percentage of the net slab weight, they required that the torque-variation rate required to explain the PA direction change reconstructed by Wessel and Kroenke (2008) be the same as that provided by subduction initiation along the Izu-Bonin-Mariana and Tonga-Kermadec trenches. Black boxes in Figure 1a mark the boundaries of the pairs (H_A, μ_A) that are compatible with both

constraints described above, when one assumes that slab pull is 20% (solid box) and 80% (dashed box) of the net slab weight. The inferred values of plausible asthenosphere viscosities, which account also for uncertainties in the duration of the bend event and the magnitude of Hawaiian plume drift (see Iaffaldano & Lambeck, 2014, for more details), are smaller if one assumes that slab pull is 20%, rather than 80%, of the net slab weight. This can be explained by recalling that if only 20%—as opposed to 80%—of the net weight of the newly subducted lithosphere along the Izu-Bonin-Mariana and Tonga-Kermadec trenches contributes to pulling the PA, then a less-viscous asthenosphere is required to balance such a force change rate and result in the PA direction change reconstructed by Wessel and Kroenke (2008). We note that within the geodynamically plausible regions of pairs (H_A, μ_A), one can constrain the pulling force with an uncertainty of less than 1 order of magnitude (Figure 1a).

This simple example demonstrates how the inference of plate-driving forces becomes much less uncertain if one considers the joint constraints on asthenospheric viscosity and thickness (Iaffaldano & Lambeck, 2014; Paulson & Richards, 2009). Accordingly, in this study, we first reevaluate the role of PA slab pull forces along the Aleutians-Japan, Marianas-Izu-Bonin, and Tonga-Kermadec trenches since the mid-Miocene, in light of these recent constraints. To complement this analysis, we also briefly review the possible Couette (passive) and Poiseuille (active) flow regimes within the asthenosphere. Finally, we resort to recently developed coupled global models of mantle and lithosphere dynamics (Stotz et al., 2017) to quantify the Poiseuille and Couette flow components beneath the PA since 15 Ma. This provides new insight into the contribution of sub-Pacific asthenospheric flow to the force-balance governing Pacific Plate motion.

2. Present-Day Slab Pull Forces Upon PA

We further develop the simple force-balance inversion presented above, in 3-D spherical geometry, with a more direct focus on the present-day PA dynamics. Specifically, we write an analytical equation for the balance of torques acting upon the PA. Such an equation includes contributions from the following: (i) slab pull along the Aleutians-Japan, Marianas-Izu-Bonin, and Tonga-Kermadec trenches; (ii) ridge push along the boundaries separating PA from Nazca (East Pacific Rise) and Antarctica; (iii) frictional resistance along all PA trenches and transform faults; and (iv) the basal drag exerted by a resisting asthenosphere. The latter term is readily calculated from the PA geometry, its stage Euler vector, the sub-Pacific asthenosphere thickness, and its viscosity. We take the present-day Euler vector from our recent reconstruction (Stotz et al., 2017), while asthenospheric viscosity and thickness are taken within the geodynamically plausible ranges shown in Figure 1a (black boxes). We calculate the torque associated with ridge-push forces using the formula of Fowler (2004), assuming that forces are directed perpendicular to the ridge axis. The torque associated with frictional forces is calculated by integrating shear stresses along convergent and transform margins of the PA. We calculate the torque associated with slab pull along the Aleutians-Japan, Marianas-Izu-Bonin, and Tonga-Kermadec trenches by integrating the linear density of slab pull force along them. We deliberately keep the pulling force densities as free parameters of the torque-balance equation as this allows us to invert the equation for their values. The equations underlying this analysis are presented in the supporting information (Bird, 1998; Buffett & Becker, 2012; Capitanio et al., 2007; Conrad, Bilek, & Lithgow-Bertelloni, 2004; Conrad & Lithgow-Bertelloni, 2002; Davies, 1999; Fowler, 2004; Iaffaldano et al., 2012; Iaffaldano & Bunge, 2015; Kohlstedt et al., 1995; Suppe, 2007).

Blue, green, and red filled areas in Figure 1b show the slab pull force required along the Aleutians-Japan, Marianas-Izu-Bonin, and Tonga-Kermadec trenches to drive the present-day PA kinematics, respectively (assuming that the underlying asthenosphere is resisting plate motion). For any value of the asthenosphere viscosity, the thickness of the box is determined from the uncertainties on the friction coefficient (in the range 0.01–0.07, see supporting information) and on the viscosity of the lower part of the upper mantle—in the range 1.4×10^{21}–4.0×10^{21} Pa·s. We calculate slab pull linear densities for values of the asthenosphere viscosity (μ_A) within the solid black box of Figure 1a, having assumed that 20% of the net slab weight contributes to pulling the trailing plate. In the supporting information we show the same analysis for values of μ_A within the dashed black box in Figure 1a (i.e., assuming that 80% of the net slab weight contributes to pulling the trailing plate). The slab pull contribution from the Marianas-Izu-Bonin subduction zone (green full area) is considerably larger than the other two (blue and red full areas) due to the position of the trenches relative to the present-day PA Euler pole (i.e., due to the direction of PA motion).

Next, we compare the estimates of slab pull linear density needed along the three PA trenches with the maximum pulling force one can possibly expect from these slabs. We do so not to infer precise values of slab pull force densities along the PA margins but, rather, to test whether the notion of PA motion being driven mainly by subduction — with the asthenosphere resisting it — remains viable in light of the aforementioned constraints on the viscosity and thickness of Earth's asthenosphere. To this end, we first integrate the density contrast between slabs and mantle over the slab volume, in order to obtain slab weights. The thickness of slabs is estimated from their age at the trench — in the range 50–140 Ma, depending on the specific trench segment (Gibbons et al., 2015) — based on the half-space cooling model (e.g., Davies, 1999). In line with previous studies, we assume that only the portion of slabs above the 660 km discontinuity contributes to pulling the trailing plate (e.g., Conrad, Bilek, Lithgow-Bertelloni, 2004; Lallemand et al., 2005; Lithgow-Bertelloni & Richards, 1998; van Summeren et al., 2012). We consider slab density contrasts ranging from 65 to 75 kg/m^3. Then, we subtract the integral of viscous stresses around slabs from their weights to obtain net slab weights. Viscous stresses are calculated assuming that slabs sink vertically into the mantle at a rate equal to the subduction velocity at the trench. Finally, we assume that only a certain percentage of the net slab weight pulls the trailing plate, with the remaining part contributing instead to bending the lithosphere at the trench (e.g., Buffett & Becker, 2012; Capitanio et al., 2007; Conrad & Hager, 1999, among others).

Results are shown in Figure 1b, where we assume that 20% of the net weight of the slab pulls the trailing plate. Blue, green, and the red transparent areas are the ranges of maximum slab pull force available along the Aleutians-Japan, Marianas-Izu-Bonin, and Tonga-Kermadec subduction zones, respectively. In the supporting information we repeat the calculation assuming that 80% of the net weight of the slab pulls the trailing plate. Both comparisons indicate that the pulling forces required along the Aleutians-Japan, Marianas-Izu-Bonin, and Tonga-Kermadec trenches in order to drive the present-day PA kinematics (filled areas) systematically exceed the maximum force exerted by sinking slabs (transparent areas). In other words, the assumption that the PA motion is mainly driven by subduction appears to be geodynamically implausible in light of the recent constraints on asthenosphere viscosity and thickness. Indeed, our calculations demonstrate that under the most favorable conditions (i.e., low asthenosphere viscosity), the maximum slab pull along the PA trenches may account for, at most, half of the PA motion (see supporting information). As a consequence, we next consider the presence of a strong driving component of flow (i.e., Poiseuille type) within the sub-Pacific asthenosphere.

3. Couette and Poiseuille Flow Regimes in the Asthenosphere

Dynamic balance (i.e., the balance of both forces and torques) within viscous fluids dictates that flow can be of two types: Couette and Poiseuille. The former arises in the absence of internal driving forces and is dictated by motion of the boundaries of the fluid environment. An example of this is laminar viscous flow within a horizontal channel between a top moving plate and a stationary bottom. Flow in the channel arises by virtue of horizontal shear stresses imposed by the moving plate and propagating vertically through the fluid. Figure 2a illustrates Couette flow generated within a 150 km thick channel by a plate moving at a horizontal velocity of 7.5 cm/yr. Since these conditions aim to approximate, to first order, those of the sub-Pacific asthenosphere, we use a fluid viscosity of $\mu_A = 5 \times 10^{19}$ Pa·s, compatible with the channel thickness, having assumed $\mu_{UM} = 1.4 \times 10^{21}$ Pa·s. These conditions imply horizontal shear stresses of around 0.8 MPa, which remain constant with depth. Poiseuille flow, on the other hand, is driven by internal forces within the fluid, in the absence of moving boundaries. Figure 2b illustrates two examples of Poiseuille flow within the above mentioned channel, in the presence of horizontal pressure gradients equal to 10 (dashed line) and 20 (solid line) Pa/m, for cases with stationary top and bottom boundaries. The resulting flow has a parabolic profile with depth, with velocities peaking in the middle of the asthenospheric channel. Solving the 1-D equation for dynamic balance yields a midchannel flow velocity $v = \Delta P/\Delta L \cdot H_A^2/(8\mu_a)$, where ΔP is the pressure difference across the channel, while ΔL is the distance over which ΔP acts. Horizontal stresses in this case are as high as 0.75 and 1.5 MPa (for low- and high-pressure gradient cases, respectively) close to the top and bottom boundaries and decrease to zero toward the channel middle depth.

Because Couette and Poiseuille flow types are independent solutions of the dynamic balance equation for viscous flow, they can occur together within Earth's asthenosphere. In fact, any asthenospheric flow pattern can be expressed as a linear combination of Couette and Poiseuille flow patterns. In Figure 2c we combine the Couette/Poiseuille patterns in Figures 2a/2b to illustrate the flow arising within the asthenospheric channel when the overlying plate moves at 7.5 cm/yr, in the presence of a horizontal pressure gradient within the asthenosphere. Solid and dashed lines refer, respectively, to the high- and low-pressure gradient cases

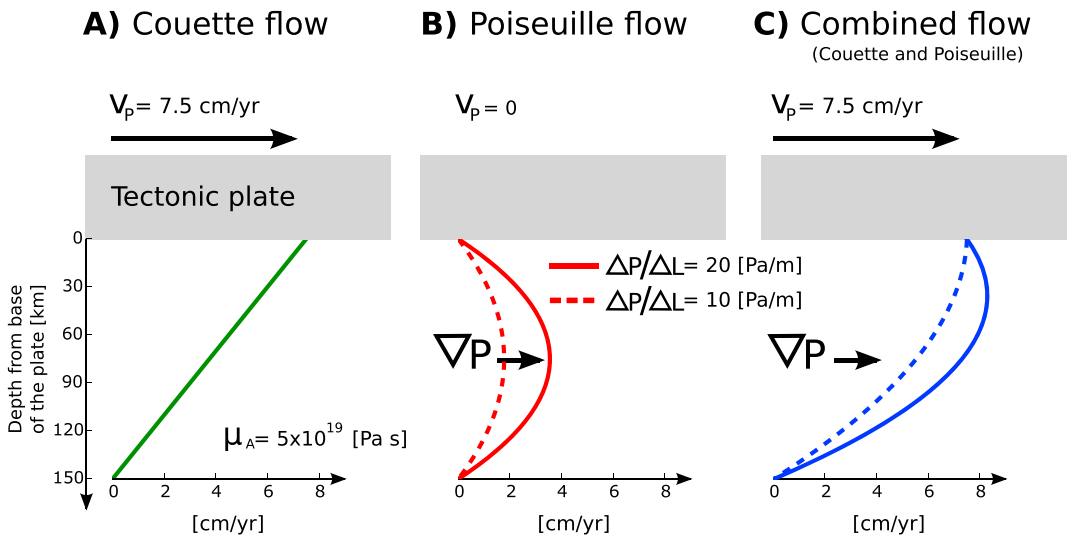

Figure 2. (a) Example of Couette flow generated within a 150 km thick channel by a plate moving at a horizontal velocity of 7.5 cm/yr; (b) example of Poiseuille flow associated with low (10 Pa/m—dashed line) and high (20 Pa/m—solid line) pressure gradients; and (c) combination of flow components in Figures 2a and 2b.

explored above. In the case of a high-pressure gradient, the asthenospheric flow exceeds the velocity of the plate at some depth (solid line). However, in the case of low-pressure gradient, flow within the channel is nowhere faster than the plate above (dashed line), despite the maximum stresses associated with Poiseuille and Couette components being similar (0.8 and 0.75 MPa). This simple example illustrates that the presence of a significant Poiseuille flow component does not necessarily imply that the asthenosphere flows faster than the overlying plate. Previous studies have attempted to quantify the Couette and Poiseuille contributions to flow within Earth's asthenosphere, via numerical simulations of viscous flow (e.g., Hoeink & Lenardic, 2010; Hoeink et al., 2011, 2012) or lithosphere dynamics (e.g., Bird et al., 2008). However, these studies did not simulate coupled global mantle and lithosphere dynamics at the convective vigor of Earth's mantle (i.e., at a Rayleigh number of 10^7–10^8), which is essential for quantifying the relative contributions of these flow regimes.

4. Poiseuille and Couette Flow Underneath PA From Coupled Global Models of Mantle and Lithosphere Dynamics

We resort to our recently published coupled global models of mantle and lithosphere dynamics (Stotz et al., 2017) to simulate PA motion since the mid-Miocene and quantify, from the resulting dynamics, the Poiseuille and Couette contributions to the sub-Pacific asthenospheric flow. Our models merge two existing numerical codes, TERRA and SHELLS, to simulate the time evolving dynamics of the coupled mantle and lithosphere system. This allows us to simultaneously account for shallow- and deep-seated contributions to the torque balance, such as the deviatoric stresses associated with lateral thickness variations of the lithosphere (including ridge push), frictional forces along plate margins, pull associated with the net weight of slabs sinking into Earth's mantle and viscous flow, at the lithosphere's base, associated with mantle convection. The details of each of these models have been previously described in a suite of publications (e.g., Baumgardner, 1985; Bird, 1998; Bunge & Baumgardner, 1995; Davies & Davies, 2009; Davies et al., 2013; Kong & Bird, 1995, among others), while the coupling strategy is reported in Stotz et al. (2017). The models presented here incorporate two important technical advances relative to our previous study: (i) slab pull forces along trenches are calculated by mapping, from the temperature field, the slab weight minus the associated shear stresses at its surface, and we assume that only 25% of the net slab weight contributes to pulling the PA; (ii) the finite-element grid for simulating global mantle flow features 0.67 billion grid points, which corresponds to a resolution of ~10 km at the surface and ~5 km at the core-mantle boundary (see supporting information for further details). This advance allows our models to resolve sharper mantle viscosity contrasts. In particular, our radial mantle viscosity profile features an asthenospheric thickness of 100–150 km,

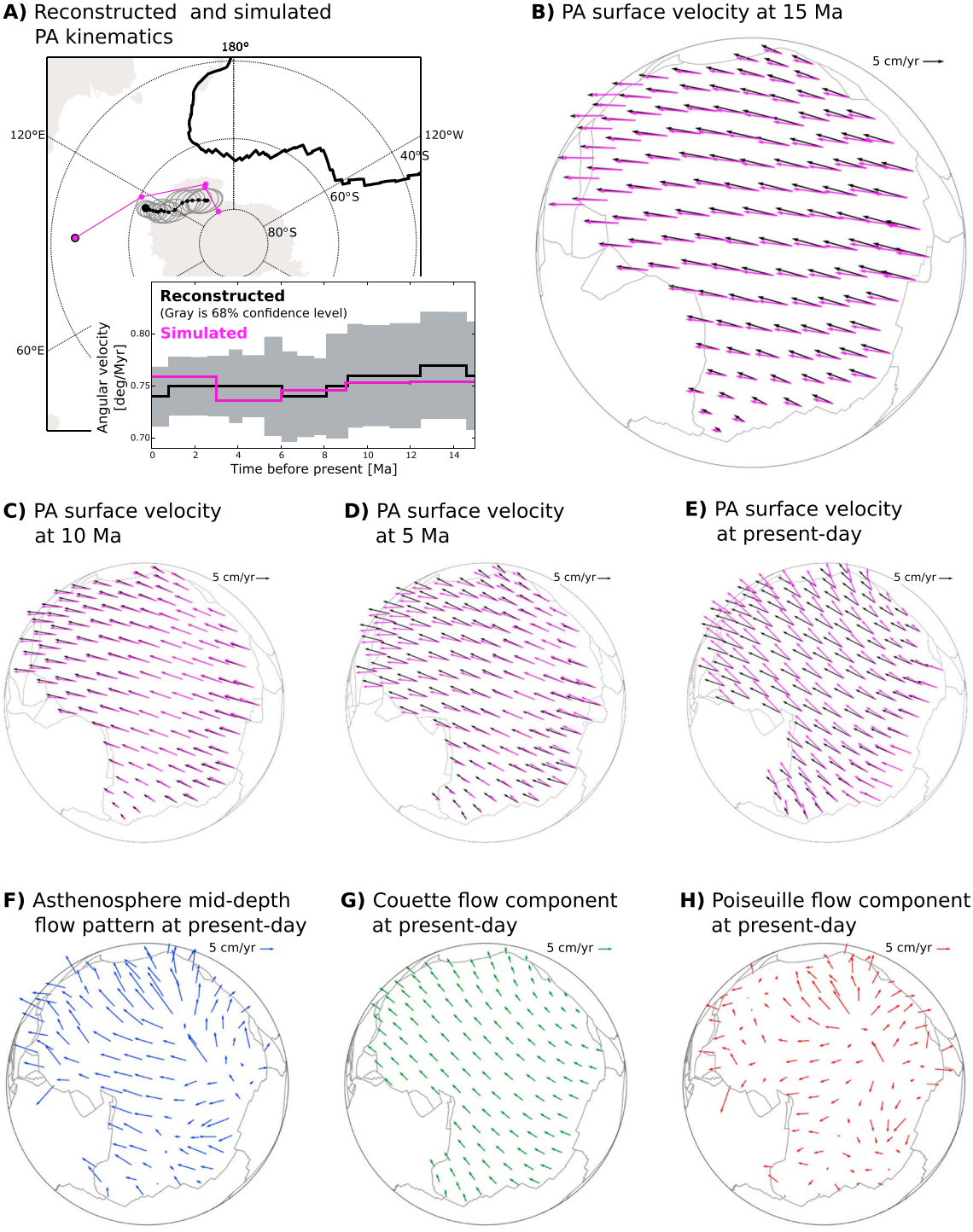

Figure 3. (a) Reconstructed (in black) and simulated (in magenta) PA kinematics since mid-Miocene. The large panel shows Euler poles (biggest dot denotes the most recent position of the Euler pole, continents are in gray, PA margins are in thick black), while the small panel shows the temporal progression of angular velocities; (b–e) reconstructed and simulated PA surface velocity at selected stages in time. Plate margins are in gray. (f) Simulated middle asthenosphere flow beneath the PA at 15 Ma; (g, h) middle-asthenosphere Couette and Poiseuille flow components, respectively, beneath the PA at 15 Ma.

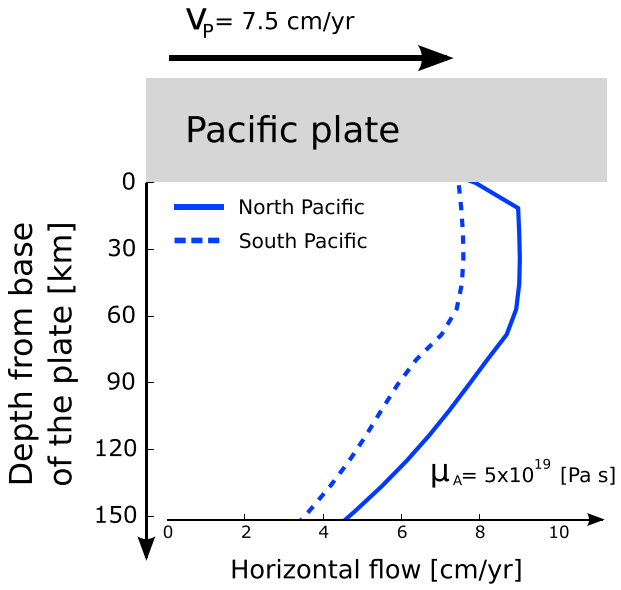

Figure 4. Vertical profile of average horizontal asthenospheric flow beneath the PA at the present-day. Solid and dashed lines refer to the northern and southern parts of the PA, respectively.

and a temperature-dependent asthenospheric viscosity that averages to 5×10^{19} Pa·s. Because of these features, the Rayleigh number associated with our simulations is Earth-like and the resulting velocities require no scaling between TERRA and SHELLS.

Figure 3a compares the PA kinematics over the past 15 Myr from our simulations with those reconstructed by Stotz et al. (2017). The main panel shows the temporal progression of reconstructed (in black) and simulated (in magenta) Euler poles, while the small panel reports the associated angular velocities. For ease of comparison, we average the simulated Euler vectors (which are output at a temporal resolution of 1 Myr—see supporting information) over 3 Myr long stages. Our simulations are capable of reproducing (i.e., within the 68% confidence interval) the time-progression of angular velocities. The reconstructed PA Euler pole wonders within the Antarctic continent over the past 15 Myr (black square is the pole for the most recent reconstructed stage), slowly migrating northwestward. Our simulated PA Euler pole fits closely the overall pattern of reconstructed poles, with the only exception being the pole associated with the most recent stage (black contoured circle), which sits within the Indian ocean instead of laying offshore Antarctica. Considering that the reconstructed PA Euler poles are ultimately constrained by just two multibeam data surveys, the first along the Pitman Fracture Zone (Cande et al., 1995) and the second along the Menard Francture Zone (Croon et al., 2008), we deem this to be a reasonable fit. Figures 3b–3e illustrate reconstructed and simulated PA surface velocities at 15, 10, 5 Ma and at the present-day, respectively.

On the basis of the fit of simulated to reconstructed kinematics, we draw inferences on the contribution of slab pull forces to the PA kinematics. Our simulations indicate that the slab pull force along the PA subduction trenches is, on average, 6×10^{12} N/m (arising from 25% of the net weight of slabs), in agreement with the maximum force estimated in Figure 1b. We use plate velocities and mantle-flow patterns from our simulations to quantify the Couette and Poiseuille components of sub-Pacific asthenospheric flow. Initially, we extract the flow field at the middle asthenospheric depth (i.e., 225 km) beneath the PA. This is shown in Figure 3f and represents the combination of both Couette and Poiseuille contributions. Next, we use the simulated surface velocities of PA to calculate the Couette component of flow at this depth (Figure 3g). Finally, we subtract the Couette flow component from the total asthenospheric flow to obtain the Poiseuille flow component (Figure 3h). This exhibits minimum and maximum velocities of ~1 and ~9 cm/yr, respectively, and an average of ~4 cm/yr (in the supporting information we present these analyses for the 5, 10, and 15 Ma stages). We also note that although the simulated PA kinematics differ slightly, the first-order patterns reported here are consistent across a number of simulations where we varied both the percentage of slab pull force contributing to pulling the PA and values for the friction coefficient along plate margins. These simulations yield similar averages of Poiseuille flow (~4 cm/yr), indicating that PA dynamics has been driven by a significant Poiseuille flow component since at least 15 Ma.

To make a simple, yet direct comparison between our results and the analytical flow solution in Figure 2c, in Figure 4 we calculate the vertical averages of horizontal flow velocities at 15 Ma underneath the northern and southern portions of the PA, up to 150 km below the base of the lithosphere. Solid and dashed lines refer to the northern and southern portions of the PA, respectively—which are representative of the fast and slow moving portions of the PA—due to their positions with respect to the PA Euler poles. Our results indicate that flow beneath the northern part of the PA is indeed faster than the PA surface velocity, buy this is not the case beneath the southern PA. We have verified that such a pattern remains consistent in our simulations since the mid-Miocene (i.e., over the past 15 Myr). As illustrated also through the simple example above (Figure 2), this indicates that the Poiseuille component of flow in the sub-Pacific asthenosphere is significant and that the associated basal shear stresses contribute strongly (at least 50%) to driving the PA motion over the past 15 Myr. In fact, since the Poiseuille flow velocity at the channel middle depth is $v = \Delta P/\Delta L \cdot H_A^2/(8\mu_A)$, an average flow of ~4 cm/yr across PA implies a pressure gradient of around 22 Pa/m. Over a distance of half the length scale of PA (around 5,000 km), this corresponds to a pressure variation of around ±55 MPa. If one wanted to search for the dynamic-topography expression of such a pressure difference, as done in recent studies

(Colli et al., 2016), then the expectation would be of finding up to ±1.6 km. This is in line with estimates based on mantle convection simulations (e.g., Flament et al., 2013, and references therein) but is somewhat higher than estimates based on seismic reflection surveys of the oceanic lithosphere (Hoggard et al., 2016).

5. Conclusions

We have reviewed recent glacial isostatic adjustment and lithosphere dynamics constraints on the viscosity and thickness of Earth's asthenosphere, and their impact on the inference of plate-driving forces. In light of these constraints, we analytically inverted the 3-D torque-balance equation and calculated the slab pull forces required along the Aleutians-Japan, Marianas-Izu-Bonin, and Tonga-Kermadec trenches to drive the present-day Pacific Plate motion entirely through subduction—with the sub-Pacific asthenosphere passively resisting this motion via a purely Couette flow component. We found that this results in unrealistically high predictions of slab pull forces, which calls for a more active role for asthenospheric flow in driving the Pacific Plate, via a strong pressure-driven Poiseuille flow component. We resorted to coupled global models of mantle and lithosphere dynamics to simulate the dynamics of the Pacific Plate over the past 15 Myr. Our output kinematics are in good agreement with recent Pacific Plate motion reconstructions. On this basis, we isolated from our modeled sub-Pacific asthenospheric flow (on average, as high as 9 cm/yr) the plate-driving Poiseuille component. We found this to be, on average, as high as 4 cm/yr and conclude that the associated shear stresses at the base of the Pacific Plate drive more than half of the Pacific Plate motion since at least 15 Ma.

Acknowledgments

All data, numerical codes, and methods used in this study come from the sources referenced or are described herein. TERRA is housed on Bitbucket and is available from the authors on request. SHELLS is available at the website http://peterbird.name/. Authors developed the numerical models presented here at the Australian National University and are grateful to the Research School of Earth Science for the environment they provided. I. L. S. acknowledges support from CONICYT Becas-Chile scholarship and from IGN at the University of Copenhagen. D. R. D. acknowledges funding from the Australian Research Council, via grants FT140101262 and DP170100058. Numerical simulations were undertaken at the NCI National Facility in Canberra, Australia, which is supported by the Australian Commonwealth Government.

References

Baumgardner, J. R. (1985). 3-dimensional treatment of convective flow in the Earth's mantle. *Journal of Statistical Physics*, *39*(5–6), 501–511.

Bird, P. (1998). Testing hypotheses on plate-driving mechanisms with global lithosphere models including topography, thermal structure, and faults. *Journal of Geophysical Research*, *103*, 10,115–10,129. https://doi.org/10.1029/98JB00198

Bird, P., Liu, Z., & Rucker, W. K. (2008). Stresses that drive the plates from below: definitions, computational path, model optimization, and error analysis. *Journal of Geophysical Research*, *113*, B11406. https://doi.org/10.1029/2007JB005460

Buffett, B. A., & Becker, T. W. (2012). Bending stress and dissipation in subducted lithosphere. *Journal of Geophysical Research*, *117*, B05413. https://doi.org/10.1029/2012JB009205

Bunge, H. P., & Baumgardner, J. R. (1995). Mantle convection modeling on parallel virtual machines. *Computational Physics*, *9*(2), 207–215. https://doi.org/10.1063/1.168525

Cande, S. C., Raymond, C. A., Stock, J., & Haxby, W. F. (1995). Geophysics of the Pitman fracture zone and Pacific-Antarctic plate motions during the Cenozoic. *Science*, *270*, 947–953.

Capitanio, F., Morra, G., & Goes, S. (2007). Dynamic models of downgoing plate-buoyancy driven subduction: Subduction motions and energy dissipation. *Earth and Planetary Science Letters*, *262*(1), 284–297. https://doi.org/10.1016/j.epsl.2007.07.039

Colli, L., Ghelichkhan, S., & Bunge, H.-P. (2016). On the ratio of dynamic topography and gravity anomalies in a dynamic Earth. *Geophysical Research Letters*, *43*(6), 2510–2516. https://doi.org/10.1002/2016GL067929

Colli, L., Stotz, I., Bunge, H. P., Smethurst, M., Clark, S., Iaffaldano, G., … Bianchi, M. C. (2014). Rapid South Atlantic spreading changes and coeval vertical motion in surrounding continents: Evidence for temporal changes of pressure-driven upper mantle flow. *Tectonics*, *33*, 1304–1321. https://doi.org/10.1002/2014TC003612

Conrad, C. P., Bilek, S., & Lithgow-Bertelloni, C. (2004). Great earthquakes and slab pull: Interaction between seismic coupling and plate-slab coupling. *Earth and Planetary Science Letters*, *218*(1–2), 109–122. https://doi.org/10.1016/S0012-821X(03)00643-5

Conrad, C. P., & Hager, B. H. (1999). Effects of plate bending and fault strength at subduction zones on plate dynamics. *Journal of Geophysical Research*, *104*(B8), 17,551–17,571. https://doi.org/10.1029/1999JB900149

Conrad, C. P., & Lithgow-Bertelloni, C. (2002). How mantle slabs drive plate tectonics. *Science*, *298*(5591), 207–209. https://doi.org/10.1126/science.1074161

Croon, M. B., Cande, S. C., & Stock, J. M. (2008). Revised Pacific-Antarctic plate motions and geophysics of the Menard fracture zone. *Geochemistry, Geophysics, Geosystems*, *9*, Q07001. https://doi.org/10.1029/2008GC002019

Davies, D. R., & Davies, J. H. (2009). Thermally-driven mantle plumes reconcile multiple hotspot observations. *Earth and Planetary Science Letters*, *278*, 50–54. https://doi.org/10.1016/j.epsl.2008.11.027

Davies, D. R., Davies, J. H., Bollada, P. C., Hassan, O., Morgan, K., & Nithiarasu, P. (2013). A hierarchical mesh refinement technique for global 3-D spherical mantle convection modelling. *Geoscientific Model Development*, *6*(4), 1095–1107. https://doi.org/10.5194/gmd-6-1095-2013

Davies, G. F. (1999). *Dynamic Earth: Plate, Plumes mand Mantle Convection*. Cambridge, UK: Cambridge University Press.

Faccenna, C., Becker, T. W., Lallemand, S., & Steinberger, B. (2012). On the role of slab pull in the Cenozoic motion of the Pacific plate. *Geophysical Research Letters*, *39*, L03305. https://doi.org/10.1029/2011GL050155

Flament, N., Gurnis, M., & Müller, R. D. (2013). A review of observations and models of dynamic topography. *Lithosphere*, *5*(2), 189–210. https://doi.org/10.1130/L245.1

Forsyth, F., & Uyeda, S. (1975). Relative importance of driving forces of plate motion. *Geophysical journal of the royal Astronomical Society*, *43*, 163–200. https://doi.org/10.1111/j.1365-246X.1975.tb00631.x

Fowler, C. M. R. (2004). *The solid Earth*. Cambridge, UK: Cambridge University Press.

French, S., Lekic, V., & Romanowicz, B. (2013). Waveform tomography reveals channeled flow at the base of the oceanic asthenosphere. *Science*, *342*, 227–230. https://doi.org/10.1126/science.1241514

Gibbons, A. D., Zahirovic, S., Müller, R. D., Whittaker, J. M., & Yatheesh, V. (2015). A tectonic model reconciling evidence for the collisions between India, Eurasia and intra-oceanic arcs of the central-eastern Tethys. *Gondwana Research*, *28*(2), 451–492. https://doi.org/10.1016/j.gr.2015.01.001

Haskell, N. A. (1937). The viscosity of the asthenoshpere. *American Journal of Science*, *33*, 22–28.

Hoeink, T., Jellinek, A. M., & Lenardic, A. (2011). Viscous coupling at the lithosphere-asthenosphere boundary. *Geochemistry, Geophysics, Geosystems*, *12*, Q0AK02. https://doi.org/10.1029/2011GC003698

Hoeink, T., & Lenardic, A. (2010). Long wavelength convection, Poiseuille-Couette flow in the low-viscosity asthenosphere and the strength of plate margins. *Geophysical Journal International*, *180*(1), 23–33. https://doi.org/10.1111/j.1365-246X.2009.04404.x

Hoeink, T., Lenardic, A., & Richards, M. (2012). Depth-dependent viscosity and mantle stress amplification: Implications for the role of the asthenosphere in maintaining plate tectonics. *Geophysical Journal International*, *191*(1), 30–41.

Hoggard, M. J., White, N., & Al-Attar, D. (2016). Global dynamic topography observations reveal limited influence of large–scale mantle flow. *Nature Geoscience*, *9*, 456–463. https://doi.org/10.1038/ngeo2709

Iaffaldano, G., Bodin, T., & Sambridge, M. (2012). Reconstructing plate-motion changes in the presence of finite-rotations noise. *Nature Communications*, *3*, 1048.

Iaffaldano, G., & Bunge, H.-P. (2015). Rapid plate motion variations: Observations serving geodynamic interpretation. *Annual Review of Earth and Planetary Science*, *43*, 571–592.

Iaffaldano, G., & Lambeck, K. (2014). Pacific plate-motion change at the time of the Hawaiian-Emperor bend constrains the viscosity of Earth's asthenosphere. *Geophysical Research Letters*, *41*, 3398–3406. https://doi.org/10.1002/2014GL059763

Karato, S. (2010). Rheology of the Earth's mantle: A historical review. *Gondwana Research*, *18*, 17–45.

Karato, S. (2012). On the origin of the asthenosphere. *Earth and Planetary Science Letters*, *321–322*, 95–103.

Kohlstedt, D. L., Evans, B., & Mackwell, S. J. (1995). Strength of the lithosphere: Constraints imposed by laboratory experiments. *Journal of Geophysical Research*, *100*, 17,587–17,602.

Kong, X., & Bird, P. (1995). SHELLS: A thin-shell program for modeling neotectonics of regional or global lithosphere with faults. *Journal of Geophysical Research*, *100*(B11), 22,129–22,131. https://doi.org/10.1029/95JB02435

Lallemand, S., Heuret, A., & Boutelier, D. (2005). On the relationships between slab dip, back-arc stress, upper plate absolute motion, and crustal nature in subduction zones. *Geochemistry, Geophysics, Geosystems*, *6*(9), Q09006. https://doi.org/10.1029/2005GC000917

Lithgow-Bertelloni, C., & Richards, M. A. (1998). The dynamics of Cenozoic and Mesozoic plate motions. *Reviews of Geophysics*, *36*, 27–78. https://doi.org/10.1029/97RG02282

Mitrovica, J. X. (1996). Haskell [1935] revisited. *Journal of Geophysical Research*, *101*(B1), 555–569. https://doi.org/10.1029/95JB03208

Paulson, A., & Richards, M. A. (2009). On the resolution of radial viscosity structure in modelling long-wavelength postglacial rebound data. *Geophysical Journal International*, *179*(3), 1516–1526. https://doi.org/10.1111/j.1365-246X.2009.04362.x

Rowley, D. B., Forte, A. M., Rowan, C. J., Glisovic, P., Moucha, R., Grand, S. P., & Simmons, N. A. (2016). Kinematics and dynamics of the East Pacific Rise linked to a stable, deep-mantle upwelling. *Science Advances*, *2*, E1601107.

Schellart, W. P. (2004). Quantifying the net slab pull force as a driving mechanism for plate tectonics. *Geophysical Research Letters*, *31*(7), L07611. https://doi.org/10.1029/2004GL019528

Seno, T. (2000). Why the Philippine Sea plate moves as it does. *Journal of the Geological Society of the Philippines*, *50*, 105–117.

Stotz, I. L., Iaffaldano, G., & Davies, D. R. (2017). Late-Miocene Pacific plate kinematic change explained with coupled global models of mantle and lithosphere dynamics. *Geophysical Research Letters*, *44*, 7177–7186. https://doi.org/10.1002/2017GL073920

Suppe, J. (2007). Absolute fault and crustal strength from wedge tapers. *Geology*, *35*(12), 1127–1130. https://doi.org/10.1130/G24053A.1

van Summeren, J., Conrad, C. P., & Lithgow-Bertelloni, C. (2012). The importance of slab pull and a global asthenosphere to plate motions. *Geochemist Geophysics Geosystems*, *13*, Q0AK03. https://doi.org/10.1029/2011GC003873

Wessel, P., & Kroenke, L. W. (2008). Pacific absolute plate motion since 145 Ma: An assessment of the fixed hot spot hypothesis. *Journal of Geophysical Research*, *113*, B06101. https://doi.org/10.1029/2007JB005499